State-space PTA

Kimpson[1], Melatos, O'Leary, Evans, others, etc. etc. ⋆ †
[1]Royal Astronomical Society, Burlington House, Piccadilly, London W1J 0BQ, UK

Last updated 17 June 2023

ABSTRACT
This is an abstract

Key words: editorials, notices – miscellaneous

1 INTRODUCTION

The inspiral of supermassive black hole binaries (SMBHBs; Rajagopal & Romani 1995; Wyithe & Loeb 2003; Sesana 2013; Ravi et al. 2015), is predicted to result in the emission of nHz gravitational waves (GWs). Other potential GW sources in this low-frequency regime include cosmic strings (e.g. Sanidas et al. 2012) and cosmological phase transitions (e.g. Xue et al. 2021). The detection of these long-wavelength GWs has necessitated the development of novel astrophysical methods, since it is practically impossible to engineer interferometric detectors with sufficiently long baselines. The foremost technique for the detection of GWs in this low-frequency regime is a via timing an ensemble of pulsars; a pulsar timing array (PTA; Verbiest et al. 2021). The presence of a nHz GW will influence the propagation of the pulsar radio beacon, leaving a characteristic impression on the received pulsar timing signal. By measuring the modulation of the pulsar signal in this way, one can effectively construct a detector with a baseline on the scale of parsecs. Multiple PTA detectors have now been built over the last few decades, including the North American Nanohertz Observatory for Gravitational Waves (NANOGrav, Arzoumanian et al. 2020), the Parkes Pulsar Timing array (PPTA Kerr et al. 2020), and the European Pulsar Timing Array (EPTA, Ferdman et al. 2010). These previously disparate efforts have now been joined in international collaboration, under the umbrella of the International Pulsar Timing Array (IPTA, Perera et al. 2019), along with a number of newer PTAs such as the Indian Pulsar Timing Array Project (InPTA, Tarafdar et al. 2022), as MeerTime (Bailes et al. 2020; Spiewak et al. 2022) and the Chinese PTA (Hobbs et al. 2019).

The incoherent superposition of multiple SMBHB sources leads to a stochastic GW background detectable at nHz frequencies (Allen 1997; Sesana et al. 2008; Christensen 2019; Renzini et al. 2022). Previous efforts have mainly focused on the detection of this stochastic background via measuring the correlation in the pulsar timing residuals between any two pair of pulsars; the presence of a GW induces a characteristic correlation as a function of the angular separation between the pulsars – the Hellings-Downs curve (Hellings & Downs 1983). However, no GW background has yet been detected (Lentati et al. 2015; Arzoumanian et al. 2018; Antoniadis et al. 2022). SMBHBs which are sufficiently massive and nearby may be individually resolvable with PTAs, allowing the very earliest stages of their evolution and coalescence to be investigated (Sesana & Vecchio 2010; Zhu et al. 2015; Babak & Sesana 2012; Ellis 2013; Zhu et al. 2016). The stochastic GW background itself may be dominated by a few individual binary sources (Ravi et al. 2012). However, as with the stochastic background, PTA observational efforts to detect individual sources have thus far been unsuccessful (Zhu et al. 2014; Babak et al. 2016; Arzoumanian et al. 2023).

The intrinsic pulsar timing noise – i.e. random, unmodelled variations in the pulse arrival time due to irregularities in the rotation of the star – has been identified as a key factor limiting the sensitivity of PTAs to GW signals (Shannon & Cordes 2010; Lasky et al. 2015; Caballero et al. 2016). This timing noise has multiple theorized causes including free precession (Kerr et al. 2015; Stairs et al. 2000), microglitches (Stairs, Lyne & Shemar Ale; Melatos et al. 2008; Espinoza et al. 2021), asteroid encounters (Shannon et al. 2013; Brook et al. 2013), glitch recovery (Johnston & Galloway 1999; Hobbs et al. 2010), fluctuations in both the internal and external stochastic torques (Cordes & Greenstein 1981; Urama et al. 2006; Antonelli et al. 2023), variations in the coupling between the stellar crust and core (Jones 1990), magnetospheric state switching (Kramer et al. 2006; Lyne et al. 2010) and superfluid turbulence (Link 2012; Melatos & Link 2014). In order to mitigate the influence of timing noise, PTAs are typically composed of millisecond pulsars (MSPs) which are known to be much more stable rotators with minimal timing noise. However, timing noise in MSPs could be a "latent" phenomenon that will emerge with the increased detector sensitivity and longer timing spans necessary to detect GWs (Shannon & Cordes 2010). In addition to the temporally uncorrelated "red" timing noise there are also secondary, white noise sources that must be considered such as phase jitter noise and radiometer noise (Cordes & Shannon 2010; Lam et al. 2019; Parthasarathy et al. 2021).

In this work we present a novel approach to PTA data analysis for individual, monochromatic, SMBHB GW sources that can self-consistently account for the intrinsic timing noise inherent to pulsar observations. We formulate PTA analysis as a state-space problem and demonstrate how to optimally estimate the state-space evolution by using a Kalman filter (Kalman 1960; Meyers et al. 2021; Melatos et al. 2021). With the tracking of the intrinsic pulsar

⋆ Contact e-mail: tom.kimpson@unimelb.edu.au
† Present address: Science magazine, AAAS Science International, 82-88 Hills Road, Cambridge CB2 1LQ, UK

state established, it is then possible to determine the presence of a GW signal in the pulsar data and infer the underlying source parameters.

This paper is organised as follows. In Section 2 we present our state-space model for the pulsar pulse frequency which is subject the influence of a GW. In Section 3 we discretise the model, develop a Kalman filter to track the state evolution and introduce how to deploy the Kalman filter in conjunction with nested sampling to estimate the system parameters and the model evidence. In Section 4 we test this new method on synthetic pulsar data. Throughout this work we adopt the natural units, with $c = G = \hbar = 1$, and a $(-,+,+,+)$ metric signature.

2 STATE-SPACE FREQUENCY MODEL

We want to formulate the PTA analysis as a state-space problem with a separation between the intrinsic pulsar state, and the measurement state recorded by an observer. For this work we will take our state variable to be the intrinsic pulsar pulse frequency $f_{\rm p}(t)$, as measured in the momentarily comoving reference frame of an observer local to the pulsar. We will take our measurement variable to be the pulsar pulse frequency that is measured by an observer at Earth, $f_{\rm m}(t)$.

2.1 Evolution of the pulsar frequency

We will take as our model of the intrinsic pulsar frequency $f_{\rm p}(t)$ a variation of the phenomenological model of Vargas & Melatos (2023). Within this model, $f_{\rm p}(t)$ evolves according to a combination of both deterministic torques (i.e. electromagnetic spin-down) and stochastic torques (i.e. 'spin wandering' or timing noise, achromatic variations in the pulse time of arrival intrinsic to the star). The deterministic torque is taken to arise from the pulsar magnetic dipole, with braking index $n = 3$ whilst the stochastic torque is a simple white noise process. Specifically, the frequency evolves according to a Ornstein-Uhlenbeck process (equivalently a Langevin equation) with a time-dependent drift parameter:

$$\frac{df_{\rm p}}{dt} = -\gamma[f_{\rm p} - f_{\rm EM}(t)] + \dot{f}_{\rm EM} + \xi(t)\,, \tag{1}$$

where $f_{\rm EM}$ is the solution of the electromagnetic spindown equation, $\dot{f}_{\rm EM}$ is the spin derivative, γ a proportionality constant that specifies the mean-reversion timescale, and $\xi(t)$ a white noise process that satisfies:

$$\langle \xi(t)\xi(t')\rangle = \sigma^2\delta(t-t')\,, \tag{2}$$

for variance σ^2. For PTA analysis, we are concerned with timescales on the order of years. Consequently, we can express the EM spindown as a simple linear relation:

$$f_{\rm EM}(t) = f_{\rm EM}(0) + \dot{f}_{\rm EM}(0)t\,. \tag{3}$$

Completely, the frequency evolution is then given by the solution of the stochastic differential equation,

$$\frac{df_{\rm p}}{dt} = -\gamma[f_{\rm p} - f_{\rm EM}(0) - \dot{f}_{\rm EM}(0)t] + \dot{f}_{\rm EM}(0) + \xi(t) \tag{4}$$

As emphasised in Vargas & Melatos (2023), this model for the frequency evolution is a phenomenological model that aims to qualitatively reproduce the typical behaviour of observed pulsars, rather than being derived from a physical model of the neutron star (e.g. a model of the neutron star crust and superfluid components Meyers et al. 2021). For our purposes of exploring the detection of GWs via a state space formulation it will prove sufficiently accurate and appropriate.

2.2 Modulation of pulsar frequency due to a GW

In the presence of a GW, the pulse frequency measured by an observer in the local neutron star reference frame is different from that measured by an observer on Earth. We will now derive the influence of the GW on the received pulse frequency.

2.2.1 Plane GW perturbation

We take a gravitational plane wave that perturbs a background Minkowski spacetime as

$$g_{\mu\nu} = \eta_{\mu\nu} + H_{\mu\nu}e^{i(\Omega(\hat{n}\cdot\bar{x}-t)+\Phi_0)}\,, \tag{5}$$

for Minkowski metric $\eta_{\mu\nu}$ with spatial coordinates $\bar{x}$, where the GW has a constant angular frequency Ω, propagates in the $\hat{n}$-direction and has a phase offset of Φ_0. We emphasise that for this work Ω has no time dependence – we are concerned solely with monochromatic sources. We are free to choose our coordinate system such that Φ_0 is the GW phase at $t = 0$ at the Earth. The amplitude tensor $H_{\mu\nu}$ has zero temporal components ($H_{0\mu} = H_{\mu 0} = 0$) whilst the spatial part is

$$H_{ij} = h_+ e^+_{ij}(\hat{n}) + h_\times e^\times_{ij}(\hat{n})\,, \tag{6}$$

where $h_{+,\times}$ are the polarisation amplitudes of the gravitational plane wave. The polarisation tensors $e^{+,\times}_{ij}$ are uniquely defined by the principal axes $\hat{k}, \hat{l}$ of the wave:

$$e^+_{ij}(\hat{n}) = \hat{k}_i\hat{k}_j - \hat{l}_i\hat{l}_j\,, \tag{7}$$

$$e^\times_{ij}(\hat{n}) = \hat{k}_i\hat{l}_j + \hat{l}_i\hat{k}_j\,. \tag{8}$$

The principal axes are in turn specified via the location of the GW source on the sky (via polar coordinate θ and azimuthal coordinate ϕ) and the polarisation angle ψ

$$\begin{aligned}\hat{k} &= (\sin\phi\cos\psi - \sin\psi\cos\phi\cos\theta)\hat{x}\\ &\quad - (\cos\phi\cos\psi + \sin\psi\sin\phi\cos\theta)\hat{y}\\ &\quad + (\sin\psi\sin\theta)\hat{z}\end{aligned} \tag{9}$$

$$\begin{aligned}\hat{l} &= (-\sin\phi\sin\psi - \cos\psi\cos\phi\cos\theta)\hat{x}\\ &\quad + (\cos\phi\sin\psi - \cos\psi\sin\phi\cos\theta)\hat{y}\\ &\quad + (\cos\psi\sin\theta)\hat{z}\end{aligned} \tag{10}$$

where e.g. $\hat{x}$ is a unit vector in the direction of the x-axis of the reference frame. The direction of GW propagation is related to the principal axes as,

$$\hat{n} = \hat{k}\times\hat{l}\,. \tag{11}$$

2.2.2 Pulse frequency as a photon

In general radio pulses from a pulsar are transmitted as an amplitude-modulated, radio-frequency carrier wave, where the carrier wave (i.e. the photon) is at typical radio frequencies of ~ GHz whilst the pulse frequency $f_p(t)$ is ~kHz. We are interested in measuring how the pulse frequency is perturbed by the presence of a GW. We define the geometric object

$$\vec{p} = \omega(1, -\bar{q}) \tag{12}$$

where ω is the angular pulse frequency ($= 2\pi f_p$) and $\bar{q}$ is the local propagation direction of the radio photon. We can identify $\vec{p}$ as the 4-momentum of the radio photon. Generally the measured frequency of a photon recorded by an observer who is travelling with 4-velocity u^μ is given by the coordinate-independent expression:

$$f = p_\alpha u^\alpha \,. \tag{13}$$

We want to relate the pulse frequencies measured in two reference frames; one at the emitter, i.e. the pulsar, and one at the observer on Earth. For pulsar observations the kinematical Doppler shifts relative to the Solar System barycentre (SSB) are corrected in the generation of a timing solution so that both the pulsar and the Earth are at rest in the global Minkowski coordinates. After these kinematical corrections we can consider both our emitter and receiver to be stationary, such that

$$u^\alpha|_{\rm emitter} = u^\alpha|_{\rm receiver} = (1, 0, 0, 0) \tag{14}$$

Consequently the measured frequency in both frames can be directly identified with the temporal component of the covariant 4-momentum,

$$f = p_t \tag{15}$$

The evolution of the pulse frequency as measured by the observer on Earth is then,

$$p_t(\tau)|_{\rm Earth} = p_t(t_0)|_{\rm source} + \int_{t=t_0}^{t=\tau} \dot{p}_t\, dt \tag{16}$$

where we use τ to denote the proper time recorded by the Earth observers clock, and the overdot denotes a derivative w.r.t. coordinate time along the geodesic t. Since the influence of the GW perturbation on $\dot{p}_t$ is small, we can relate the source emission and receiver times as $t_1 = t_0 + d$ and consider the photon trajectory to be an unperturbed path.

2.2.3 *Hamiltonian Mechanics*

The Hamiltonian in covariant notation can be written as

$$H = \frac{1}{2} g_{\mu\nu} p^\mu p^\nu, \tag{17}$$

which if we substitute in our expression for the perturbed metric is

$$H = \frac{1}{2}\eta_{\mu\nu} p^\mu p^\nu + \frac{1}{2} H_{ij} p^i p^j e^{i(\Omega(\bar{n}\cdot\bar{x} - t) + \Phi_0)} \tag{18}$$

Now, Hamilton's equations are

$$\frac{dx^\mu}{d\lambda} = \frac{\partial H}{\partial p_\mu}, \quad \frac{dp_\mu}{d\lambda} = -\frac{\partial H}{\partial x^\mu} \tag{19}$$

for affine parameter λ. The derivative of the temporal component of the covariant momenta is then,

$$\frac{dp_t}{d\lambda} = -\frac{i\Omega}{2} H_{ij} p^i p^j e^{i(\Omega(\bar{n}\cdot\bar{x} - t) + \Phi_0)} \tag{20}$$

The derivative w.r.t coordinate time t is

$$\dot{p}_t = \frac{dp_t}{d\lambda}\left(\frac{dt}{d\lambda}\right)^{-1} = \frac{dp_t}{d\lambda}\left(\frac{1}{p^t}\right) \tag{21}$$

Note that $\dot{p}_t$ is entirely a function of the GW perturbation. In the Minkowski case the spacetime is stationary and so p_t should be conserved along the geodesic. It will prove useful to recognise that

$$p^\mu = \omega(1, -q^x, -q^y, -q^z) \tag{22}$$

where $\bar{q}$ is the unit vector between the Earth and pulsar and ω is the *constant* photon angular frequency. Given the small effect of the GW perturbation, at first order we can identify ω as either the frequency at source or observer. Similarly, we can parameterize the photon spatial coordinates $\bar{x}$ as,

$$\bar{x}(t) = -\bar{q}(t - t_1) \tag{23}$$

Note that when our integration variable $t = t_1$ (i.e. the photon is at Earth) then $\bar{x}(t = t_1) = 0$ which is what we expect given our chosen coordinate system. Also note that $\dot{p}_t$ is entirely a function of the GW perturbation. In the Minkowski case the spacetime is stationary and so p_t should be conserved along the geodesic. We will treat the pulsar locations to be constant with respect to the Earth, i.e. $\bar{q}$ is not a function of time. In practice, the pulsar locations vary with respect to the Earth, but are constant with respect to the solar system barycentre (SSB). This barycentering correction is typically applied during the pulsar detection process. Our conclusions are generally unchanged by this choice - it is straightforward to transform q if needed into a vector between the SSB and pulsar.

Bringing this all together we can write $\dot{p}_t$ in a condensed form as,

$$\dot{p}_t = A e^{iBt + C} \tag{24}$$

with

$$A = -\frac{i\Omega\omega}{2} H_{ij} q^i q^j \tag{25}$$

$$B = -\Omega(1 + \bar{n}\cdot\bar{q}) \tag{26}$$

and

$$C = \Omega\tau\bar{n}\cdot\bar{q} + \Phi_0 \tag{27}$$

From Eq 16 the frequency shift experienced by the observer relative to the source due to a GW is then

$$p_t(\tau)|_{\rm Earth} - p_t(\tau - d)|_{\rm source} = \tag{28}$$

$$A\int_{t=\tau-d}^{t=\tau} e^{iBt+C}\, dt \tag{29}$$

$$= \frac{-iA}{B} e^{i(-\Omega\tau + \Phi_0)}\left(1 - e^{-iBd}\right) \tag{30}$$

$$= \frac{\omega}{2}\frac{h_{ij}(\tau; \bar{x} = 0) q^i q^j}{(1 + \bar{n}\cdot\bar{q})}\left(1 - e^{i\Omega(1+\bar{n}\cdot\bar{q})d}\right) \tag{31}$$

for $h_{ij} = g_{ij} - \eta_{ij}$. Since via Equation 13 we can related the temporal component of the covariant momentum to the frequency, it follows that

$$f(\tau)|_{\rm Earth} = f(\tau - d)|_{\rm source}\left(1 - \frac{\omega}{2}\frac{h_{ij}(\tau; \bar{x} = 0) q^i q^j}{(1 + \bar{n}\cdot\bar{q})}\left(1 - e^{i\Omega(1+\bar{n}\cdot\bar{q})d}\right)\right) \tag{32}$$

where we have identified ω with $f(\tau - d)|_{\rm source}$.

3 DETECTION AND PARAMETER ESTIMATION

Let's review and categorise all the free parameters,$\bar{\theta}$, of above model. We can generally separate these into parameters which correspond to the intrinsic frequency evolution of the pulsar and parameters of the GW source

$$\bar{\theta} = \bar{\theta}_{\rm PSR} \cup \bar{\theta}_{\rm GW} \tag{33}$$

$$\bar{\theta}_{\rm PSR} = [\gamma, f_{\rm EM}(0), \dot{f}_{\rm EM}(0), d]^{(N)} \tag{34}$$

$$\bar{\theta}_{\rm GW} = [h_+, h_\times, \delta, \alpha, \psi, \Omega, \Phi_0] \tag{35}$$

Whilst the GW parameters are shared between measurements for each pulsar, the pulsar parameters are clearly not. For a PTA dataset of N pulsars we have $7+5N$ parameters to estimate. Note that whilst this is a large parameter space, in general the pulsar parameters are much better constrained than the GW parameters: for example we have rough estimates for the pulsar distances accurate to $\sim 10\%$, but we have no prior information on the source location.

wave which are given by

$$h_+ = h(1+\cos^2\iota) \tag{36}$$

$$h_\times = -2h\cos\iota \tag{37}$$

In this section we present a new method to infer the model parameters and calculate the marginal likelihood (i.e. the model evidence). In Section 3.1 we will present a discretised version of the model of Section 2 which maps onto the discretely sampled observable $f(\tau)|_{\rm Earth}$. In Section 3.2 we will outline how observations of this pulse frequency can be used to recover the underlying intrinsic pulsar state $f(\tau - d)|_{\rm source}$ using a Kalman Filter. In Section 3.3 we will demonstrate how to deploy the Kalman filter in conjunction with a nested sampling technique to recover the model parameters. We will now review the Kalman filter and the associated likelihood in Section 3.2 before going on in Section 3.3 to discuss how to use nested sampling methods together with the filter for detection (model selection) and parameter estimation.

3.1 Discretised model

We can express the intrinsic frequency evolution, Eq. 4, in a alternative form as,

$$df = \mathcal{A}f\,dt + N(t)dt + \sigma dB(t) \tag{38}$$

where $\mathcal{A} = -\gamma$, $N(t) = \gamma(f_{\rm EM}(0) + \dot{f}_{\rm EM}(0)t) + \dot{f}_{\rm EM}(0)$ and $dB(t)$ denotes increments of Brownian motion (Wiener process). This equation is easily identified as an Ornstein-Uhlenbeck process which has a general solution given by (Gardiner 2009),

$$f(t) = e^{\mathcal{A}t}f(0) + \int_0^t e^{\mathcal{A}(t-t')}N(t')dt' + \int_0^t e^{\mathcal{A}(t-t')}\sigma dB(t') \tag{39}$$

If we move from a solution in continuous time, t, to discrete time, $\bar{t} = (t_1, t_2, ..., t_K)$, then

$$f(t_{i+1}) = Ff(t_i) + T_i + \eta_i \tag{40}$$

where

$$F_i = e^{\mathcal{A}(t_{i+1}-t_i)} \tag{41}$$

$$T_i = \int_{t_i}^{t_{i+1}} e^{\mathcal{A}(t_{i+1}-t')}N(t')dt' \tag{42}$$

$$\eta_i = \int_{t_i}^{t_{i+1}} e^{\mathcal{A}(t_{i+1}-t')}\sigma dt' \tag{43}$$

if we specialise to the case of constatn time sampling

The discrete solution $f(\bar{t})$ to the intrinsic frequency can be related to the discrete measured frequency via Eq. 32 as,

$$f_M(\bar{t}) = f(\bar{t})g(\bar{\theta}, \bar{t}) + N_M \tag{44}$$

where $g(\theta, t)$ can be expressed in a trigonometric form as

$$X = 1 - \frac{1}{2}\frac{H_{ij}q^iq^j}{(1+\bar{n}\cdot\bar{q})}\left[\cos(-\Omega\tau + \Phi_0) - \cos(-\Omega\tau + \Phi_0 + \Omega(1+\bar{n}\cdot\bar{q})d)\right] \tag{45}$$

whilst N_M is a Gaussian measurement noise that satisfies

$$\langle N_M(t)N_M(t')\rangle = \Sigma^2\delta(t-t') \tag{46}$$

for variance Σ^2.

3.2 Kalman Filtering

The Kalman filter (Kalman 1960) is a algorithmic technique for recovering a set of system state variables, $\bar{x}$, given some noisy measurements, $\bar{z}$. It is a common technique in signal processing that has also been applied more recently with great success in astrophysics (e.g. Meyers et al. 2021; Melatos et al. 2021). The linear Kalman filter operates on measurements that are related to states via a linear transformation

$$\bar{z} = \bar{H}\bar{x} + \bar{v} \tag{47}$$

where $\bar{H}$ is the measurement matrix and $\bar{v}$ a Gaussian measurement noise. The underlying states are the solutions to the state-space equation

$$\dot{\bar{x}} = \bar{F}\bar{x} + \bar{G}\bar{u} + \bar{w} \tag{48}$$

for the system dynamics matrix,$\bar{F}$, control model G, control vector $\bar{u}$, and w a stochastic zero-mean process. By comparison with the preceding equations, Eqs. 38 - **??**, it is immediately obvious how our state space model maps onto the Kalman filter structure. Specifically, our states are just the N intrinsic pulsar frequencies $\bar{x} = (f_1, f_2, ...f_N)$ whilst our measurements are the N measured pulse frequencies $\bar{z} = (f_1^{(M)}, f_2^{(M)}, ...f_N^{(M)})$. If we specialize to the case of constant time sampling between our observations, Δt, then for our formulation the components that make up the Kalman filter are as follows:

$$F_i = F_{i+1} = e^{-\gamma\Delta t} \tag{49}$$

$$T_i = \int_{t_i}^{t_{i+1}} e^{A(t_{i+1}-t')}N(t')dt' \tag{50}$$

$$= f_{\rm EM}(0) + \dot{f}_{\rm EM}(0)(\Delta t + t_i) - e^{-\gamma\Delta t}(f_{\rm EM}(0) + \dot{f}_{\rm EM}(0)t_i) \tag{51}$$

$$H_i = 1 - A(\theta_{\rm GW})\cos(-\Omega t_i(1+n\cdot q) + \Phi_0) \tag{52}$$

where the i subscript labels the value at the i-th timestep, and A is a constant that is given by Eq. **??**.

The Kalman filter includes the effect of process noise $\bar{w}$ and the measurement noise $\bar{v}$ via the definition of a process noise matrix $Q = E[ww^T]$ and a measurement noise matrix $R = E[vv^T]$, which have the discrete form,

$$Q_i\delta_{ij} = \langle\eta_i\eta_j^T\rangle = \frac{-\sigma^2}{2\gamma}\left(e^{-2\gamma\Delta t} - 1\right) \tag{53}$$

$$R_i = R_{i+1} = \Sigma^2 \tag{54}$$

The above equations, Eqs. 49 - 54, apply to an operation on a single state. The extension to N states is straightforward, since one just needs to construct a diagonal matrix for each of the Kalman

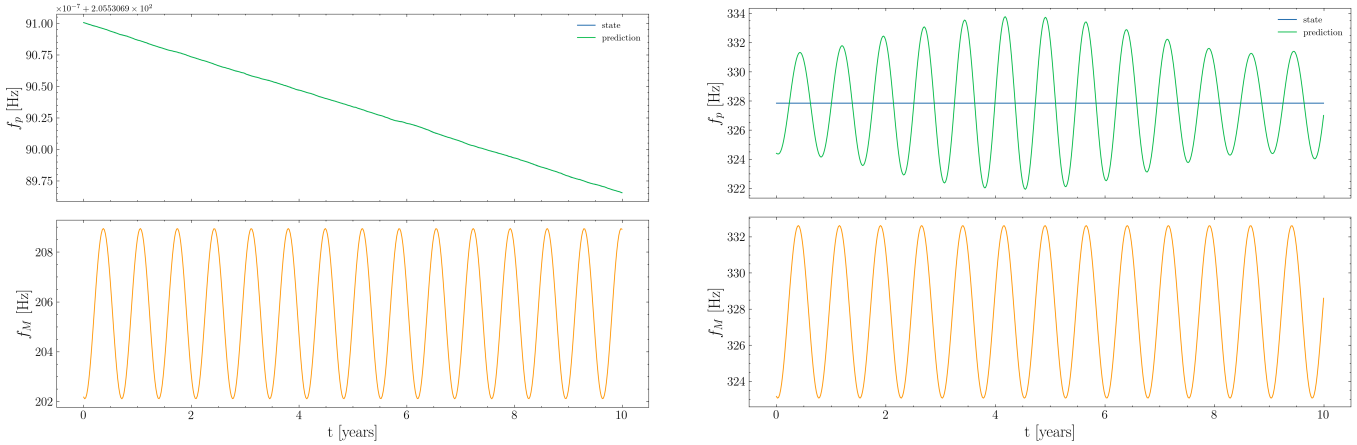

(a) Using correct parameters

(b) Using incorrect parameters

Figure 1. Application of a Kalman filter to recover the intrinsic frequency states (top panels) given a measured frequency signal (bottom panels) which has been modulated by the presence of a gravitational wave. In the case where the parameters of the filter are accurate (subfigure (a)) the underlying states are also recovered accurately. Conversely, when the parameters fed to the filter are inaccurate (subfigure (b)) the filter cannot recover the state. TK: this needs to be just one stacked figure.

components where each non-zero element corresponds to a separate pulsar frequency. For our formulation we are concerned only with the linear Kalman filter since the measurements are a linear function of the states and the state transitions are also linear. Extension to non-linear problems is straightforward using either an extended Kalman filter (Zarchan & Musoff 2000), the unscented Kalman filter (Wan & Van Der Merwe 2000) or the particle filter (Simon 2006). For a full review of the Kalman filter equations in an astrophysical context, which may be unfamiliar to some, we refer the reader to the appendices of Melatos et al. (2021) and Meyers et al. (2021).

In order for the Kalman filter to function successfully, the parameters of the model, which appear in the various Kalman matrices, must be accurate. Erroneous or inaccurate parameters lead to inaccurate predictions of the underlying states (e.g. Fig 1). The filter tracks the error in its predictions of the underlying states by projecting the state predictions back into measurement space, $\hat{x} \rightarrow \hat{z}$. These measurement predictions can then be compared against the true observed measurements i.e. $\epsilon = \bar{z} - \hat{z}$. The Gaussian log-likelihood at timestep i, as a function of the parameters is,

$$\log \mathcal{L}_i = -\frac{1}{2}(N \log 2\pi + \log\det|S_i| + \epsilon_i^T S_i^{-1} \epsilon_i) \tag{55}$$

where S_i is the covariance matrix of the error ϵ_i. The net log-likelihood is simply the sum over all timesteps.

3.3 Nested Sampling

Nested Sampling (Skilling 2006) is an integration algorithm used for evaluating integrals of the Bayesian evidence form,

$$Z = \int \mathcal{L}\pi(\theta) d\theta \tag{56}$$

where $\pi(\theta)$ is the prior which is a function of a set of unknown parameters θ. The primary advantage of nested sampling is the ability to compute this evidence integral, which is key for model selection, and proves difficult without considerable extra cost for the usual Markov Chain Monte Carlo (MCMC) approaches. Nested sampling is also typically less computationally intensive than MCMC and can handle multi-modal problems (Ashton et al. 2022). For these reasons, it has enjoyed widespread adoption in the physical sciences, particularly within the cosmological community (Mukherjee et al. 2006; Feroz & Hobson 2008; Handley et al. 2015), but has also commonly been applied in astrophysics (Buchner 2021), particle physics (Trassinelli 2019) and materials science (Pártay et al. 2009). Within this work we also use nested sampling for parameter estimation and model selection.

Multiple nested sampling libraries exist. For gravitational astrophysics it is common to use the dynesty sampler CITE, via the Bilby gravitational wave inference library and we continue to follow this precedent. TK: we may end up not even using Bilby/dynesty so leaving this section unfilled for now. Do we need a very short description of how nested sampling works?

3.4 Practical considerations

heterodyeing

pulsar terms For now we will consider the measurement noise to be known, although in principle this too could be estimated.

4 TESTS WITH SYNTHETIC DATA

We go on to discuss our choice of pulsars to make up our PTA in Section 4.1, before deploying these techniques in Sections 4.2 , 4.3 for parameter estimation and model selection.

4.1 PTA pulsars

With our Kalman filter and nested sampling techniques in hand, in order to proceed it is necessary to specify a PTA configuration. As discussed, multiple separate PTA detectors exist under the umbrella of the IPTA. Going forward we will take the 47 pulsars that make up the NANOGrav PTA (Arzoumanian et al. 2020). NANOGrav is selected simply as a well-representative example of the typical pulsars that make up a PTA. Our results and formulation are not contingent on the choice of PTA, and naturally extend to other PTAs

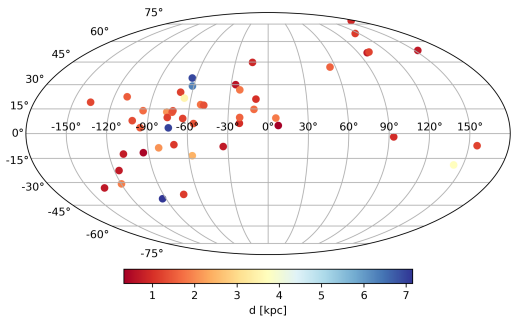

Figure 2. Spatial distribution and distances of NANOGrav pulsars

Parameter	Value
ω	5×10^{-7}
α	1.0
δ	1.0
ψ	2.50
ι	1.0
Φ_0	0.20
h	1e-2
$\sigma_{\rm p}$	10^{-13}
$\sigma_{\rm m}$	10^{-10}
T_{obs}	10 years
Δt	7 days

Table 1. GW parameters used for generating synthetic data. There is nothing special about these parameters - they are just chosen arbitrarily.

or PTAs with more pulsars.

Within our state-space formulation, the pulsar evolution is governed by a set of 5 parameters, $\bar{\theta}_{\rm PSR}$ for each pulsar. The parameters $f_{\rm EM}(0), \dot{f}_{\rm EM}(0)$ and d are well specified via existing pulsar datasets. We take the frequency and frequency derivative as returned from the pulsar datasets to simply be the values now at $t = 0$. The pulsar distances are also known, though less well constrained. Going forward we take the distances retuned from the datasets as the true values of the pulsars that make up our synthetic PTA. The specification of γ and σ are more involved. γ specifies an effective timescale of reversion to the mean TK: Need some discussion and though on how to choose these two parameters to be astrophysically reasonable c.f. A. Vargas

4.2 Parameter estimation

We are now in a position to try to infer the parameters of a GW system. We take our NANOGrav PTA and create a synthetic noisy dataset using the parameters described in Table 1. Given this synthetic data, we can try to use our KF + NS approach to recover some of the parameters. The results for inference on 5 parameters, $\omega.\Phi_0, \psi, \iota, h$ are shown in Fig 3. TK: likelihood plots for each parameter could also be of interest to include here? Need to expand this section greatly for more astrophysical systems and more unknown parameters

4.3 Detection

In addition to estimating the parameters of the system, we are also interested in how detectable a GW is using PTA + state space method. We can use our state-space tools to try to solve the problem of GW detection with a PTA i.e. *"Is there evidence of a GW in my data?"*We can frame this as a model selection procedure where we have two models/hypotheses:

- Null Model, M_0. There is no GW in the data. In this case the measurement model of the Kalman filter simply returns the frequency states i.e. $g(t, \theta) = 0$
- Alternative model, M_1. There is a GW in the data. The measurement model uses the full expression for $g(t, \theta)$

In order to accept the alternative hypothesis M_1 over M_0 there are two approaches we could take:

(i) The first is a fully Bayesian search over all the parameters for each model, calculating the evidence for each model and then determining the Bayes ratio. This is perhaps the most consistent way, but it is obviously expensive and at this stage we are keen to explore how detectability varies with e.g. GW strain.

(ii) The second method is to recognize that M_0 and M_1 are hierarchically nested models and we can perform a likelihood ratio test. That is, given the maximum likelihood estimators $\hat{\theta}$ of the true parameters θ, the likelihood of each model can be calculate. These likelihoods are just point estimates of the Bayes factor numerator/denominators. They can then be compared via the likelihood ratio Λ.

Given the cheap cost we proceed with the second method. For the likelihood ratio test we do not perform any kind of maximum likelihood search over the parameters for each of the models. Instead we just artificially set the maximum likelihood estimators to be equal to the true parameters of the system i.e. $\hat{\theta} = \theta$. We assume that any maximum likelihood algorithm would converge to these parameters. This is obviously an oversimplification but will serve our purposes for now.

Interpreting the likelihood ratio Λ also needs some consideration, since we have to account for the increased model complexity of M_1. Bayes factors penalise complexity by construction since one must integrate over a larger parameter space. There are many different ways to do this - fot now we will consider two: Akaike information criterion (AIC) and Wilks Theorem. For the latter, Wilks' Theorem which states that for a large number of samples [1] the distribution of the test statistic approaches the chi-squared distribution under the null hypothesis i.e.

$$2 \log \Lambda \rightarrow \chi^2 \tag{57}$$

One can then compute p-values where the number of degrees of freedom is equal to the difference in the number of parameters of the two models; M_1 has 7 extra parameters over M_0 corresponding to the 7 parameters of $\bar{\theta}_{\rm GW}$. With 7 degrees of freedom and a target tolerance of 5(1) % the test statistic is $\sim$ 14(18.5).

An alternative approach is to use the AIC which is given by,

$$\text{AIC} = 2k - 2 \log \mathcal{L} \tag{58}$$

where k is the number of degrees of freedom. The AIC can be computed for each model and the model with the minimum AIC is preferred. This can be straightforwardly mapped into a relative condition

$$\log \mathcal{L}_1 - \log \mathcal{L}_0 > 7 \tag{59}$$

[1] What counts as large? See https://www.osti.gov/servlets/purl/1529145

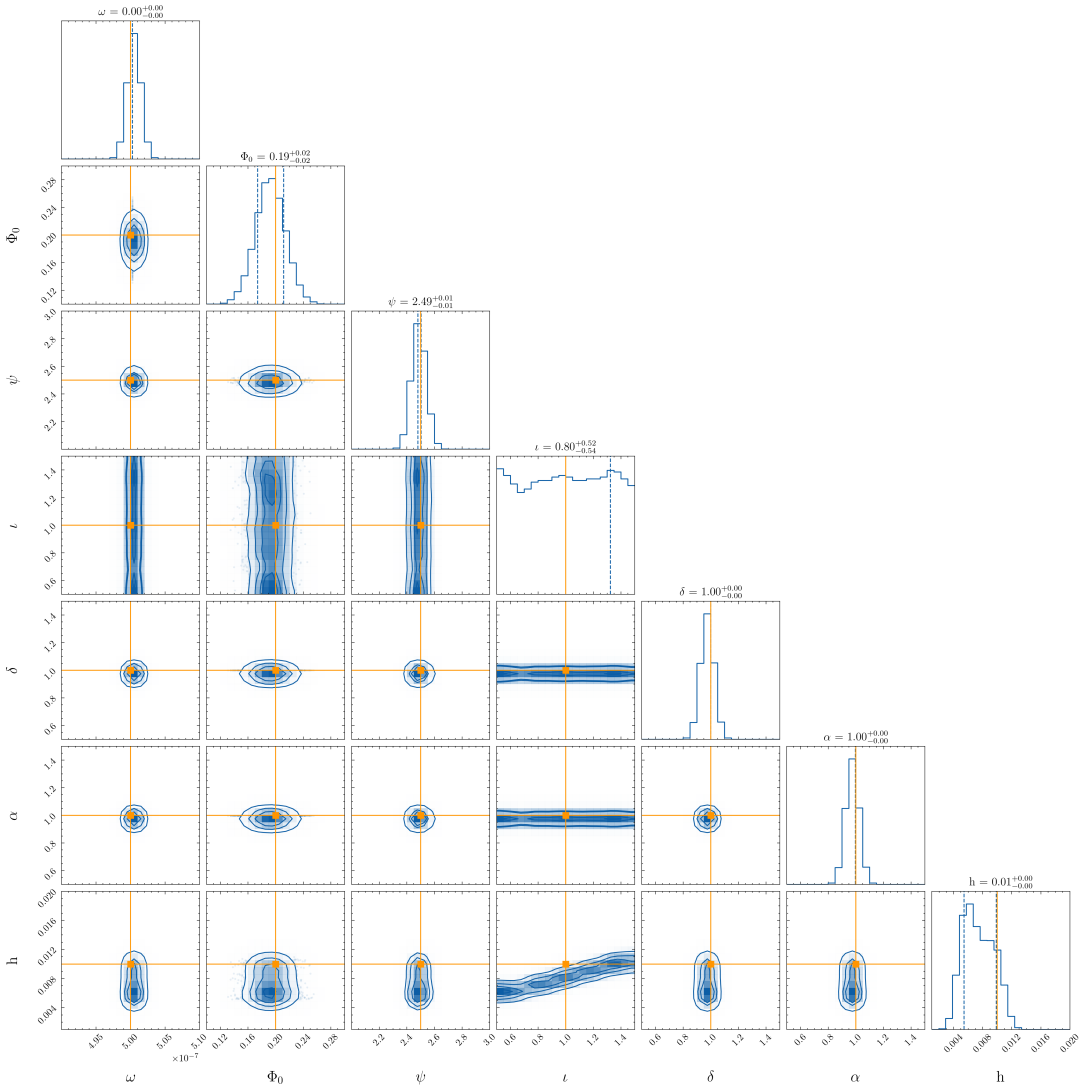

Figure 3. Example corner plot. Aside: for this run the σ_p value fed to the filter is different from that used to generate the data.

Note this is the same as the Wilks case!

5 DISCUSSION

Points to discuss:

- Non constant time sampling? Different pulsars sampled at different times...

6 CONCLUSION

Questions

- PTAs like MSPs for small timing noise. Can we get away with large timing noise, and use more pulsars? Some pulsars are more useful than others, e.g. arXiv 2211.03201
- Can we also estimate radiometer noise? Is this useful?

6.1 References

REFERENCES

Allen B., 1997, in Marck J.-A., Lasota J.-P., eds, Relativistic Gravitation and Gravitational Radiation. pp 373–417 (arXiv:gr-qc/9604033), doi:10.48550/arXiv.gr-qc/9604033

Antonelli M., Basu A., Haskell B., 2023, MNRAS, 520, 2813

Antoniadis J., et al., 2022, MNRAS, 510, 4873

Arzoumanian Z., et al., 2018, ApJ, 859, 47

Arzoumanian Z., et al., 2020, ApJ, 905, L34

Arzoumanian Z., et al., 2023, arXiv e-prints, p. arXiv:2301.03608

Ashton G., et al., 2022, Nature Reviews Methods Primers, 2, 39

Babak S., Sesana A., 2012, Phys. Rev. D, 85, 044034

Babak S., et al., 2016, MNRAS, 455, 1665

Bailes M., et al., 2020, Publications of the Astronomical Society of Australia, 37, e028

Brook P. R., Karastergiou A., Buchner S., Roberts S. J., Keith M. J., Johnston S., Shannon R. M., 2013, The Astrophysical Journal Letters, 780, L31

Buchner J., 2021, The Journal of Open Source Software, 6, 3001

Caballero R. N., et al., 2016, MNRAS, 457, 4421

Christensen N., 2019, Reports on Progress in Physics, 82, 016903

Cordes J. M., Greenstein G., 1981, ApJ, 245, 1060

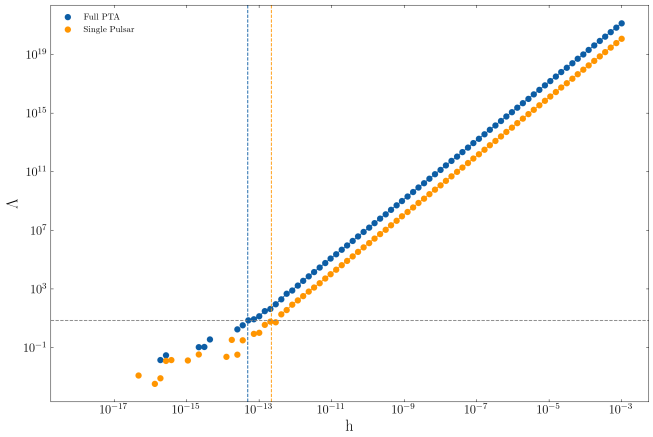

Figure 4. Likelihood ratio vs strain for *(a)* full PTA and *(b)* a single randomly chosen pulsar. Horizontal dashed line shows the minimum detectable cutoff, vertical dashed lines are the corresponding GW strains.

Cordes J. M., Shannon R. M., 2010, arXiv e-prints, p. arXiv:1010.3785
Ellis J. A., 2013, Classical and Quantum Gravity, 30, 224004
Espinoza C. M., Antonopoulou D., Dodson R., Stepanova M., Scherer A., 2021, A&A, 647, A25
Ferdman R. D., et al., 2010, Classical and Quantum Gravity, 27, 084014
Feroz F., Hobson M. P., 2008, MNRAS, 384, 449
Gardiner C., 2009, Stochastic Methods: A Handbook for the Natural and Social Sciences. Springer Series in Synergetics, Springer Berlin Heidelberg, https://books.google.com.au/books?id=otg3PQAACAAJ
Handley W. J., Hobson M. P., Lasenby A. N., 2015, MNRAS, 450, L61
Hellings R. W., Downs G. S., 1983, ApJ, 265, L39
Hobbs G., Lyne A. G., Kramer M., 2010, MNRAS, 402, 1027
Hobbs G., Dai S., Manchester R. N., Shannon R. M., Kerr M., Lee K.-J., Xu R.-X., 2019, Research in Astronomy and Astrophysics, 19, 020
Johnston S., Galloway D., 1999, Monthly Notices of the Royal Astronomical Society, 306, L50
Jones P. B., 1990, MNRAS, 246, 364
Kalman R. E., 1960, Journal of Basic Engineering, 82, 35
Kerr M., Hobbs G., Johnston S., Shannon R. M., 2015, Monthly Notices of the Royal Astronomical Society, 455, 1845
Kerr M., et al., 2020, Publ. Astron. Soc. Australia, 37, e020
Kramer M., Lyne A. G., O'Brien J. T., Jordan C. A., Lorimer D. R., 2006, Science, 312, 549
Lam M. T., et al., 2019, ApJ, 872, 193
Lasky P. D., Melatos A., Ravi V., Hobbs G., 2015, MNRAS, 449, 3293
Lentati L., et al., 2015, MNRAS, 453, 2576
Link B., 2012, Monthly Notices of the Royal Astronomical Society, 422, 1640
Lyne A., Hobbs G., Kramer M., Stairs I., Stappers B., 2010, Science, 329, 408
Melatos A., Link B., 2014, MNRAS, 437, 21
Melatos A., Peralta C., Wyithe J. S. B., 2008, ApJ, 672, 1103
Melatos A., O'Neill N. J., Meyers P. M., O'Leary J., 2021, MNRAS, 506, 3349
Meyers P. M., O'Neill N. J., Melatos A., Evans R. J., 2021, MNRAS, 506, 3349
Mukherjee P., Parkinson D., Liddle A. R., 2006, ApJ, 638, L51
Pártay L. B., Bartók A. P., Csányi G., 2009, arXiv e-prints, p. arXiv:0906.3544
Parthasarathy A., et al., 2021, MNRAS, 502, 407
Perera B. B. P., et al., 2019, MNRAS, 490, 4666
Rajagopal M., Romani R. W., 1995, ApJ, 446, 543
Ravi V., Wyithe J. S. B., Hobbs G., Shannon R. M., Manchester R. N., Yardley D. R. B., Keith M. J., 2012, ApJ, 761, 84
Ravi V., Wyithe J. S. B., Shannon R. M., Hobbs G., 2015, MNRAS, 447, 2772
Renzini A. I., Goncharov B., Jenkins A. C., Meyers P. M., 2022, Galaxies, 10, 34
Sanidas S. A., Battye R. A., Stappers B. W., 2012, Phys. Rev. D, 85, 122003
Sesana A., 2013, Classical and Quantum Gravity, 30, 224014
Sesana A., Vecchio A., 2010, Phys. Rev. D, 81, 104008
Sesana A., Vecchio A., Colacino C. N., 2008, Monthly Notices of the Royal Astronomical Society, 390, 192
Shannon R. M., Cordes J. M., 2010, ApJ, 725, 1607
Shannon R. M., et al., 2013, The Astrophysical Journal, 766, 5
Simon D., 2006, Optimal State Estimation: Kalman, H Infinity, and Nonlinear Approaches. Wiley-Interscience, USA
Skilling J., 2006, Bayesian Analysis, 1, 833
Spiewak R., et al., 2022, Publ. Astron. Soc. Australia, 39, e027
Stairs I. H., Lyne A. G., Shemar S. L., 2000, Nature, 406, 484
Tarafdar P., et al., 2022, Publications of the Astronomical Society of Australia, 39, e053
Trassinelli M., 2019, Proceedings, 33
Urama J. O., Link B., Weisberg J. M., 2006, MNRAS, 370, L76
Vargas A., Melatos A., 2023, TBD, 1, 1
Verbiest J. P. W., Osłowski S., Burke-Spolaor S., 2021, in , Handbook of Gravitational Wave Astronomy. p. 4, doi:10.1007/978-981-15-4702-7_4-1
Wan E., Van Der Merwe R., 2000, in Proceedings of the IEEE 2000 Adaptive Systems for Signal Processing, Communications, and Control Symposium (Cat. No.00EX373). pp 153–158, doi:10.1109/ASSPCC.2000.882463
Wyithe J. S. B., Loeb A., 2003, ApJ, 590, 691
Xue X., et al., 2021, Phys. Rev. Lett., 127, 251303
Zarchan P., Musoff H., 2000, Fundamentals of Kalman Filtering: A Practical Approach. Progress in astronautics and aeronautics, American Institute of Aeronautics and Astronautics, https://books.google.com.au/books?id=AQxRAAAAMAAJ
Zhu X. J., et al., 2014, MNRAS, 444, 3709
Zhu X.-J., et al., 2015, Monthly Notices of the Royal Astronomical Society, 449, 1650
Zhu X.-J., Wen L., Xiong J., Xu Y., Wang Y., Mohanty S. D., Hobbs G., Manchester R. N., 2016, Monthly Notices of the Royal Astronomical Society, 461, 1317

This paper has been typeset from a TEX/LATEX file prepared by the author.

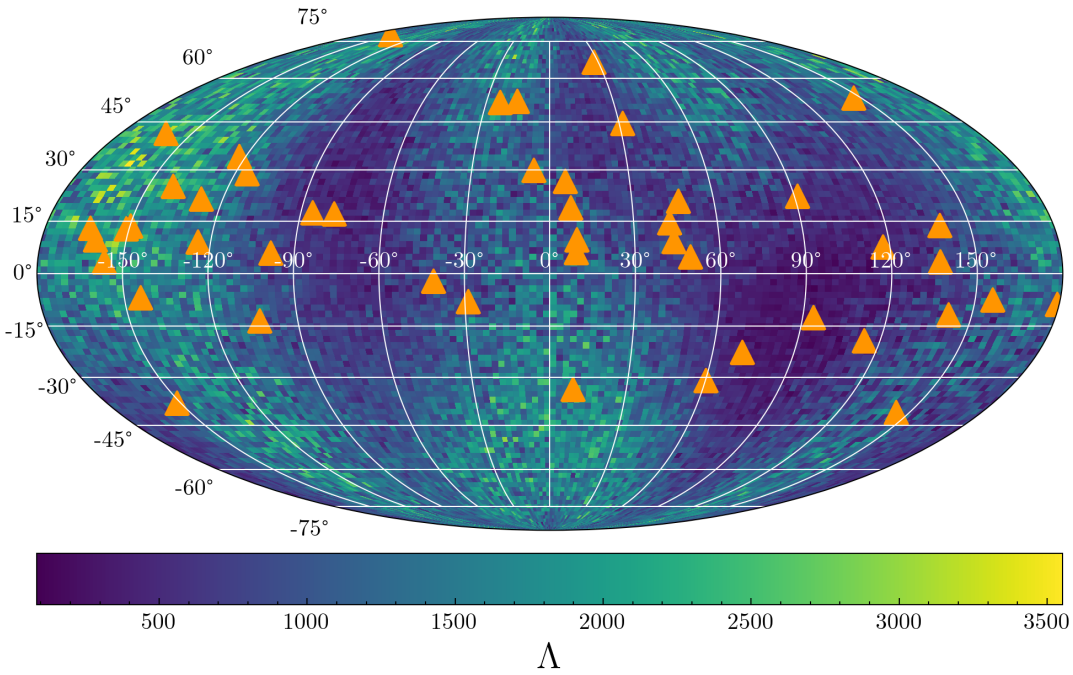

Figure 5. TK: Just a placeholder. Likelihood ratio for a given h. Maybe more interesting, but more expensive, to get minimum detectable h?